Available online at www.sciencedirect.com
SCIENCE DIRECT®
Journal of Nuclear Materials 336 (2005) 194–200
journal of nuclear materials
www.elsevier.com/locate/jnucmat

Stresses, strains and cracks in a helium-implanted SiC/C composite

J. Chen [1], P. Jung *, H. Ullmaier

Institut für Festkörperforschung, Association EURATOM-FZJ, Forschungszentrum Jülich, D-52425 Jülich, Germany

Received 18 June 2004; accepted 21 September 2004

Abstract

Helium was implanted at room temperature and at 1000 °C into $3 \times 3\,mm^2$ bars of a SiC/C particulate composite, uniformly to depths of 117 and 254 μm, respectively. Profilometry showed strong bending of the bars due to volume expansion in the implanted layer, which is ascribed to concurrently produced displacement defects. For uniform helium concentrations above ≈350 appm in layers of 254 μm thickness, scanning electron microscopy revealed spontaneous cracking just below the implanted region where tensile stress was maximum, while this critical concentration was above ≈700 appm for the 117 μm implanted layer. Below these critical concentrations the influence of helium on strength of the material was studied by 3-point bending tests. In a detailed analysis of the dependence of cracking on specimen geometry and applied stress, internal stresses from volume expansion were included. This analysis indicated hardening by implantation, in contrast to the apparent reduction of strength. The dose and temperature dependence of volume expansion was fitted by a defect recovery model.

1. Introduction

SiC-base ceramics are considered for armour or structural material of the first wall of future fusion reactors. Their major advantages are high temperature strength, acceptable thermal shock resistance and potential for low nuclear activation. In the tokamak TEXTOR at FZ-Jülich a SiC/C particulate composite was considered for armour material, combining high thermal shock resistance and moderately low atomic number Z. The slightly higher average Z as compared e.g. to Be or graphite is possibly beneficial in terms of radiative cooling of the plasma boundary layer. An important question for using these materials in fusion reactors is their resistance to radiation damage, i.e. displacement and transmutation effects. Helium may enter plasma-facing materials from three different sources:

(1) thermalised α-particles from the hot plasma (≈10^8 K) with energies below 10 keV, having ranges of about 0.1 μm in SiC,
(2) α-particles from (D, T)-reactions with maximum energies of 3.5 MeV, penetrating to a range up to ≈10 μm, and
(3) helium produced in the bulk by (n, α)-type reactions with energies around 5 MeV.

* Corresponding author. Tel.: +49 2461 614 036; fax: +49 2461 614 413.
E-mail address: p.jung@fz-juelich.de (P. Jung).
[1] Present address: Labor für Werkstoffverhalten, Paul Scherrer Institut, CH-5232 Villigen, Switzerland.

0022-3115/$ - see front matter © 2004 Elsevier B.V. All rights reserved.
doi:10.1016/j.jnucmat.2004.09.014

While the last process produces a virtually homogeneous concentration of helium, implantation by the other two processes is confined to a narrow surface layer. Measurements of helium desorption from implanted graphite [1,2] and silicon carbide [2] indicate that even at 1000 °C, the mobility of helium in both materials is still limited. This may cause retention and consequently sizeable helium inventories with consequences on material properties. In addition, the built-up of significant inhomogeneous concentrations of helium can produce internal stresses, which may affect the integrity of materials [3]. It was the aim of the present investigation to determine the effect of concentration and distribution of implanted helium on dimension and strength of a SiC–C composite material.

2. Experimental details

The material (SiC30) used in the present investigation, supplied by Schunk Kohlenstofftechnik GmbH, is a particulate composite of silicon carbide and graphite with an overall density of 2.65 g/cm^3. The supplier quotes a composition of 60 wt% SiC and $\leqslant$5 wt% free Si, balance graphite, while our chemical analysis gave 36.7 at.% Si and 63.3 at.% C. Transmission electron microscopy (TEM) showed mostly ß-SiC, some grains of C, and a few of Si, with C and Si grains always separated by SiC. The graphite was partially amorphous while the free silicon was crystalline. This structure, including the partial amorphousity of graphite, was not altered by implantation. The specimens were in the form of $101 \times 3 \times 3$ mm^3 bars with 0.3 mm of the edges truncated to avoid preferential sites for crack initiation, see Fig. 1. For implantation at ambient temperature, the specimens were mounted on water-cooled copper blocks using Wood's metal (50% Bi, 26% Pb, 13% Sn, 11% Cd, $T_{\text{melt}} \approx 71$ °C) for thermal contact. With an average power flux density of 1 MW/m^2, and assumed values for thermal conductivity (5 W/K m) and thickness (100 μm) of the Wood's metal layer, a lower limit of the temperature increase in the SiC–C specimen of 12.5 °C is estimated. Careful handling ensures that also during subsequent unmounting the temperature of 71 °C is not significantly exceeded.

The SiC/C specimens were also implanted at 1000 °C to simulate the helium effects introduced by (n,α)-reactions in a structure operating at high temperatures. Implantation was performed at the Compact Cyclotron of Forschungszentrum Jülich, using an α-beam of 26.3 MeV passing through a 25 μm Hastelloy window and a degrader wheel with 51 aluminium foils of variable thickness to give homogeneous implantation up to depths of about 117 and 254 μm, respectively, as derived from Monte Carlo calculations using TRIM95 [4]. The

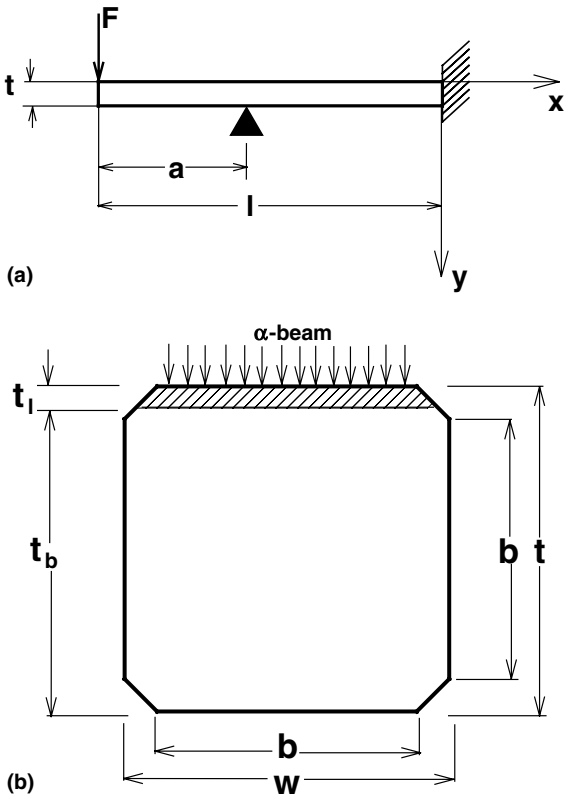

Fig. 1. (a) Schematic view of the 3-point bending device, with $a = 45$ mm and $l = 101.2$ mm. (b) Cross-section of the specimens, with $t = w = 3.00$ mm, $b = 2.41$ mm, and implantation depth t_l.

dose was measured electrically on the holder and concentrations were calculated using an average atomic density (Si + C) of the matrix of 9×10^{28} atoms/m^3. Typical particle fluxes of 5×10^{17} He/m^{2}s gave implantation rates around 0.03 appm He/s. Two specimens were mounted in parallel, thermally isolated from the specimen holder and were heated by the α-beam. A heat shield with a window of 10×12 mm^2 was mounted between degrader wheel and specimens to reduce radiation heating of the degrader wheel. The temperature of the specimens was monitored by infrared pyrometry.

After implantation the specimens were investigated by profilometry (DEKTAK^{3}ST®), by analytical scanning electron microscopy (SEM), and were fractured in an automatic 3-point bending apparatus. For technical reasons, i.e. to possibly allow operation of the device in the SEM, the bending drive and the force measurement were on opposite sides of the bar which was supported asymmetrically at a distance of 45 mm from one end (see Fig. 1(a)). The fracture surfaces were also analysed by SEM and some specimens for transmission electron microscopy (TEM) were prepared from the

implanted regions. Electron beam diffraction and microchemical analysis (EDX) were used for characterising individual grains and grain boundaries.

3. Results

3.1. Before implantation

The apparent fracture stress σ_B^* under 3-point bending is given by

$$\sigma_B^* = \frac{F \cdot a \cdot t}{2 \cdot I}, \tag{1}$$

with F, a and t defined in Fig. 1 and $I = \frac{w \cdot t^3}{12} - \frac{w-b}{t-b} \cdot \left(\frac{t^4}{16} - \frac{t^3 \cdot b}{12} + \frac{b^4}{48}\right)$ the momentum of inertia. The deflection is given by

$$y(l) = \frac{F \cdot a \cdot (1-a)^2}{3 \cdot E \cdot I}, \tag{2}$$

with E = Young's modulus. The survival function $s(\sigma_i) = (n+1-i)/(n+1)$ of an ordered sequence of n measured values $\sigma_i (i = 1, \ldots, n)$ can be described by a Weibull expression $s = \exp(-\ln 2 \cdot (\sigma_i/\sigma_0)^m)$, where σ_0 and m are average bending strength and Weibull parameter, respectively. Data for unimplanted specimens, tested at various temperatures are given in Fig. 2. A few specimens showed much lower fracture stresses than the Weibull distribution derived from the other specimens, probably due to cracks produced during preparation.

The parameters σ_0 and m derived from the plots in Fig. 2 are given as a function of temperature in Fig. 3.

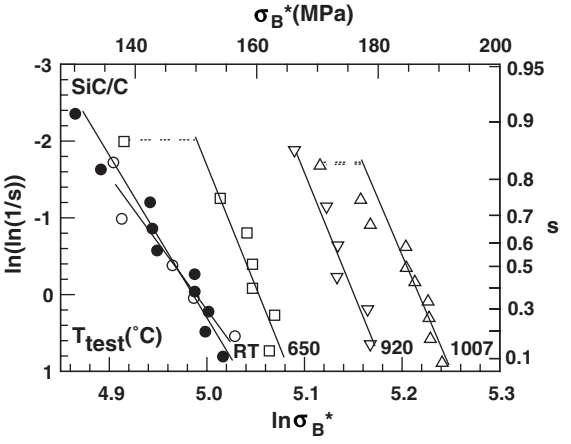

Fig. 2. Weibull plot of apparent bending strength σ_B^* of SiC/C in air at room temperature (●) and in vacuum at RT (○), 650 °C (□), 920 °C (▽) and 1007 °C (△), respectively.

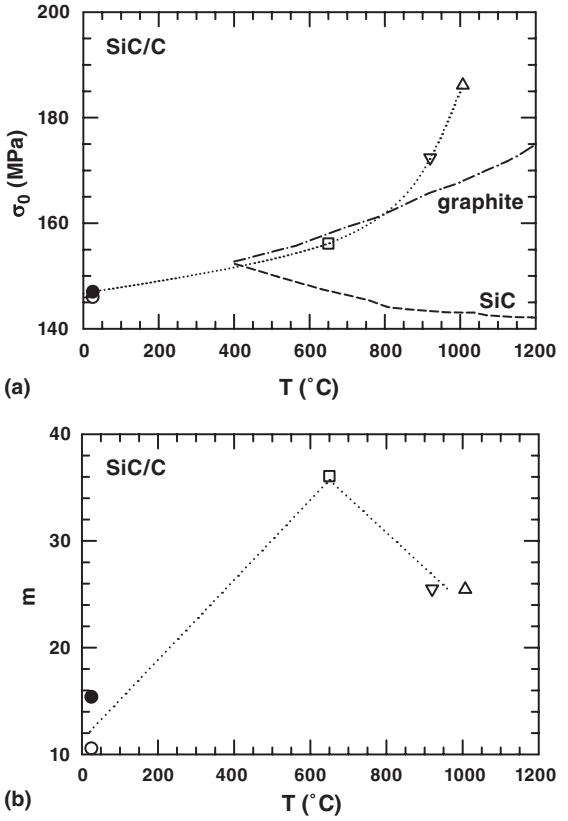

Fig. 3. Temperature dependence of average bending strengths σ_0 (a) and Weibull parameters m (b) of SiC/C from measurements in air (●) and vacuum (○). Dotted lines are included to guide the eye. The behaviour of σ_0 in pure SiC (–) [11] and in graphite (- · -) [5], normalised at 400 °C, is included for comparison.

The increase of σ_0 with temperatures corresponds to the behaviour typical for graphite [5], while the strength of pure SiC would decrease with temperature [11]. This implies that the strength of the composite is determined by rupture in the graphite grains. The absolute value of bending strength of the SiC/C composite at room temperature (148 MPa, cf. Fig. 2) is slightly lower than the value given by the supplier (190 MPa) and lies between the values of graphite (<100 MPa) [6,7] and SiC (>270 MPa) [7–10]. The values of Weibull parameters slightly exceed data in literature which range from 9.5 for graphite [7] to 9–12 [8] and 14.1 [7] for pure SiC, indicating good quality of the composite.

3.2. After implantation

After implantation the specimens revealed bending, which is schematically shown in Fig. 4 and is ascribed to volume expansion in the implanted layer. Bending angles (Fig. 5) derived from profilometry allow to obtain

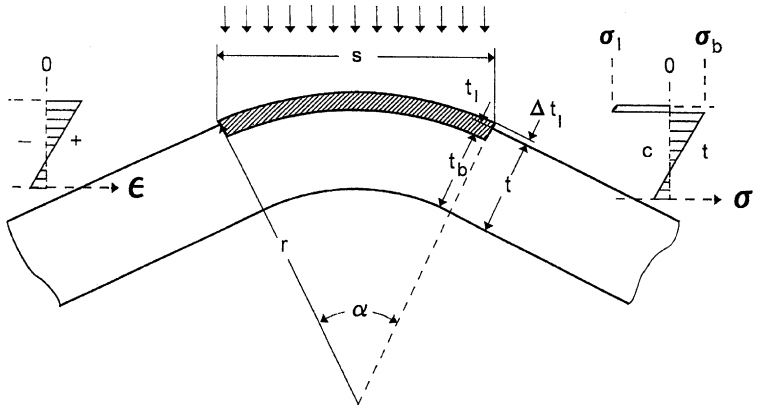

Fig. 4. Schematic view of a bar specimen, bended by homogeneous implantation in a thin layer (hatched). Inserts show actual strain and stress distributions in the central part of the specimen.

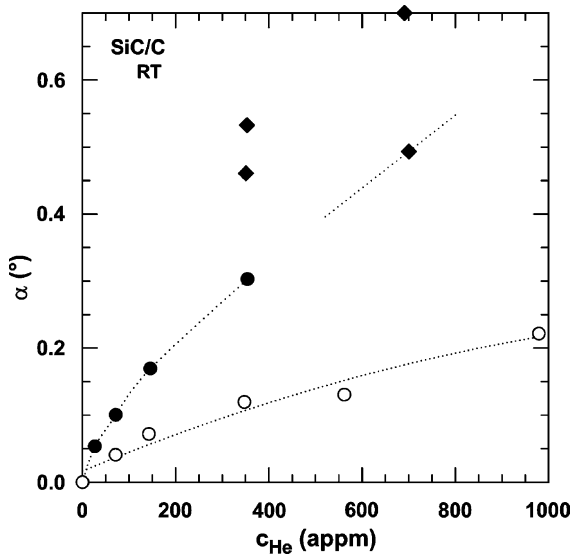

Fig. 5. Bending angles α (see Fig. 4) of SiC/C bars after implantation below 70 °C with $s = 6$ mm and $t_l = 117$ μm (○) and 254 μm (●), respectively. Included are specimens implanted to 254 μm which showed cracks, visible by SEM (◆). Dotted lines are included to guide the eyes.

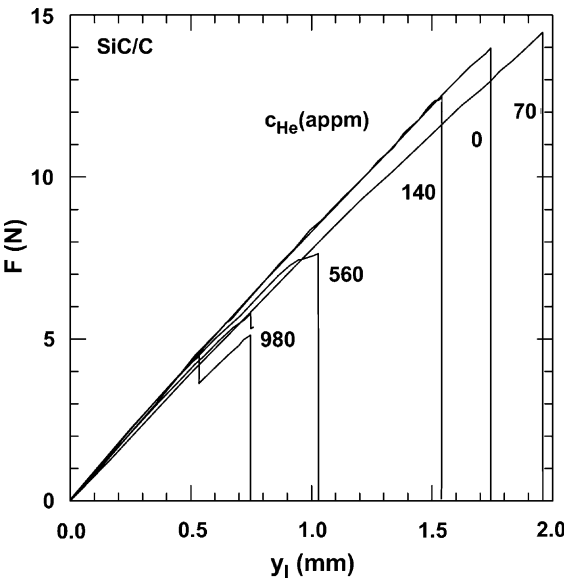

Fig. 6. Load–deflection curves of SiC/C during 3-point bending after homogeneous implantation of helium below 70 °C to a depth of 117 μm and to concentrations as indicated. The second 980 appm specimen was stopped after the first drop (crack initiation) for SEM investigation.

internal stresses (see Section 4.2). Load–deflection curves from 3-point bending tests after homogeneous helium implantation into a 117 μm layer are shown in Fig. 6. At concentrations above about 140 appm, loads give increasingly clear drop before failure. This is due to the opening of cracks below the implanted layer as shown in Fig. 7. For consistency, the loads at the drops were used for the analysis. Some of the specimens implanted to concentrations above ≈700 appm He already fractured during unmounting from the specimen holder which was ascribed to spontaneous crack formation.

The bending strengths of implanted specimens is shown in Fig. 8. At low helium concentrations the compressive stresses in the implanted region cause the fracture to shift to the unimplanted area, i.e. the difference between the maximum stress in the centre and the decreasing stress in the off-centre region during 3-point bending is overcompensated by the compressive stresses, or possibly increased strength, due to implantation. Only specimens are included in Fig. 8 which ruptured in the implanted area. At higher helium concentrations

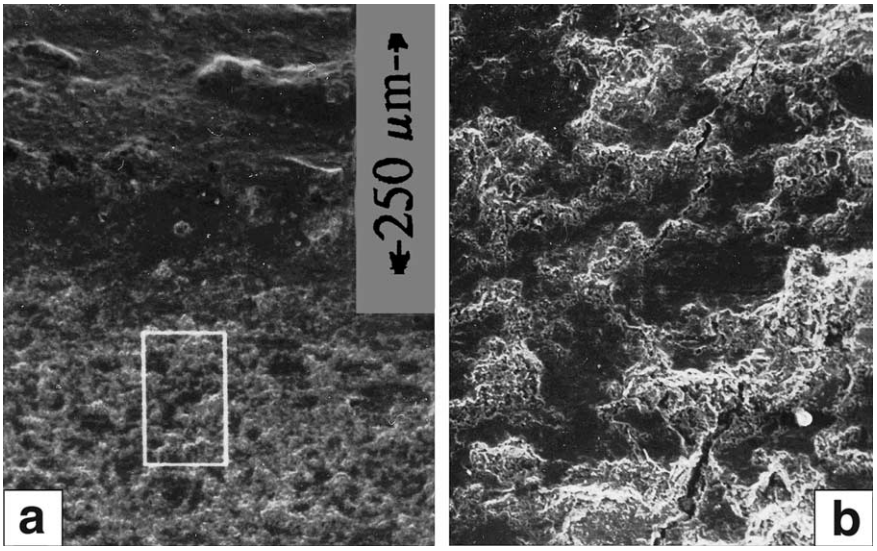

Fig. 7. Lateral view by SEM of SiC/C implanted to 700 appm He below 70 °C, showing the ≈250 μm deep implanted region (a) and an enlarged view of a crack, extending from the implanted/unimplanted interface into the unimplanted bulk (b).

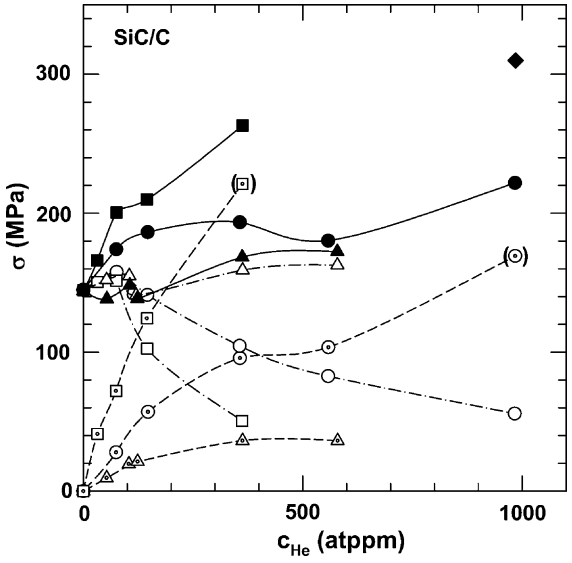

Fig. 8. Measured apparent bending strengths (σ_B^*, open symbols) of SiC/C specimens, implanted with helium below 70 °C to depths of 117 μm (○) and 254 μm (□), and at 1000 °C to 254 μm (△), respectively. Only specimens fractured in the implanted area are considered. Dotted symbols give internal stresses (σ_b) at the interface derived from equation (3). Filled symbols give true failure stresses at the interface ($\sigma_B = \sigma_B^* + \sigma_b$). One data point (◆) gives an upper estimate of σ_B in the implanted region (<70 °C, 254 μm).

the apparent bending strength decreases. These values must be corrected for internal stresses as will be discussed below.

4. Discussion

4.1. Stresses

The experimental bending strengths σ_B^* (open symbols in Fig. 8) do not reflect the real strength of the material as the interface at the upper side of the unimplanted bulk, where cracking starts, is already under tensile stress caused by the volume expansion of the implanted layer. This tension stress can be estimated from the deflection angle α derived by profilometry, cf. Ref. [12]. The radius of curvature r of the implanted part of length s (≈6 mm) of the bar is given by: $r \approx s/\alpha$. The tension stress σ_b at the upper end of the unimplanted bulk of the rectangular bar is given by

$$\sigma_b = \frac{E}{1-\nu} \cdot \frac{2 \cdot t_b}{3 \cdot r}, \tag{3}$$

with Poisson's number ν and t_b defined in Figs. 1 and 4. The strains derived from Eq. (2) yield on the average $E = 106$ GPa, virtually independent of implantation (while the supplier quotes a Young modulus of ≈140 GPa). σ_b is given by the dotted symbols in Fig. 8, using $E = 106$ MPa and $\nu = 0.25$. Addition of σ_b to the measured apparent fracture stress σ_B^* gives the true failure stresses σ_B (solid symbols in Fig. 8). σ_B^* from Eq. (1) was corrected by factors $(1 - 2t_1/t)$ to account for the slightly lower stress at the interface. Obviously only up to concentrations of about 150 appm He, the total strength is increasing and remains practically constant at higher concentrations. Above ≈350 appm, the stress measurements on the 254 μm implanted specimens are in any case uncertain, due to spontaneous crack

formation, while for the 117 μm implantation this limit is above 700 appm. The truncated edges of the present specimens cause deviations from equation (3) in the 10% range as derived from finite element calculations [13]. Fracture strengths σ_B in Fig. 8 reflect the material behaviour below the implanted layer. The fact that the strengths are somewhat above the value before implantation when cracking starts at the surface, may be ascribed to some constraints, when the crack has to open at the interface. At least at the two highest doses in Fig. 6 it is seen that complete fracture only occurs at higher stress (and strain) after crack formation at the interface. An upper limit of the strength of the implanted layer can be given, if it is assumed that the specimen is only supported by the implanted part, when a crack starts below t_1 and extends into the unimplanted region. For the present geometry its fracture strength σ_{Bi} can be approximated by $\sigma_{Bi} = F \cdot a/b \cdot t \cdot t_1$. With a more precise calculation for the maximum load (behind the drop) of the 980 appm specimen in Fig. 6, Eq. (1) gives a fracture stress in the implanted region of $\sigma_{Bi} = 311$ MPa (♦ in Fig. 8). This value is an upper limit, indicating that also in this layer only minor strengthening, if any, occurs by implantation. On the other hand, this analysis does not include possible stress enhancement by the existence of cracks in the unimplanted region. Comparison to literature data is difficult as material and experimental parameters are too different and/or data reporting or analysis is incomplete. For example a 38% decrease of bending strength was quoted in Ref. [14] after implantation of 2500 appm helium in SiC/SiC composites of 1.2 mm thickness to half depth. In this study, internal stresses were not monitored and no corrections were applied. Also no direct comparison is possible to studies where cracking was induced by coalescence of helium bubbles in neutron-irradiated B_4C [15] and BeO [16], or by different swelling of SiC versus free Si in commercial SiC [10].

Bending strengths σ_B can be related to σ_{UTS} from tensile tests for Weibull-distributed fracture probabilities by [17]

$$\sigma_B = \sigma_{UTS} \cdot (2 \cdot (m+1)^2)^{1/m}, \tag{4}$$

if deformed volumes in both cases are comparable. This gives ratios σ_B/σ_{UTS} of 1.52 and 1.33 for $m = 15$ and 25 (see Fig. 3), respectively. For comparison, an experimental ratio of 1.4 was found for Mo alloys, before and after irradiation in the Rotating Target Neutron Source II at LLNL Livermore [18].

4.2. Strains

From the bending angles in Fig. 5, linear strains ε_0 resulting from volume expansions $\Delta V/V = 3 \cdot \varepsilon_0$ can be derived (Fig. 4):

$$\varepsilon_0 = \frac{\Delta V}{3V} = \frac{t^2}{6 \cdot r \cdot t_l (1 - t_l/t)}. \tag{5}$$

Lateral strains ε_0 can be compared to a step heights Δt_1 at the border of the implanted region. For a 700 appm specimen, $\Delta t_1 \approx 3$ μm was obtained for $t_1 = 254$ μm , corresponding to a relative thickness strain $(\Delta t_1/t_1)/\varepsilon_0 \approx 1.8$, in good agreement with the value derived from analysis: $(\Delta t_1/t_1)/\varepsilon_0 \approx (1+\nu)/(1-\nu) \approx 1.7$ (for $t_1 \ll t$ and assuming isotropic lateral stresses, $\sigma_{xx} = \sigma_{yy}$). The determination of strain from bending is superior to a step height measurement, which has limited resolution due to the surface roughness (here ≈1 μm). This limitation prevents measurements below about 700 appm, while measurements at higher concentrations are not representative as cracking occurs. For comparison in Ref. [14], a volume strain of 2.1% and $(\Delta t_1/t_1)/\varepsilon_0 \approx 4.5$ were observed after implantation of 2500 appm He to a depth of ≈600 μm in 1.2 mm SiC/SiC corresponding to a damage of 0.5 dpa.

According to Eq. (5) the bending angles in Fig. 5 of about 0.12° and 0.3° at 400 appm give $\Delta V/V$ values of 1.4% (117 μm) and 1.7% (254 μm), respectively, corresponding to about 3800% per unit concentration. This value is far above unity, indicating that it cannot be ascribed to the implanted He atoms. The concurrent production of displacement defects was calculated by TRIM95 [4], using average displacement energies $T_d = 38.5$ eV [19] and binding energies $E_b = 2$ eV. A more detailed analysis in this composite material would have to include the displacement processes of each species in each component, which is not possible at the present state of knowledge. Average defect production in units of displacements per atom (dpa) is $Kt \approx 81 \cdot c_{He}$ for maximum implantation depth of 117 μm and $99 \cdot c_{He}$ for 254 μm, with defect production decreasing by about a factor of 2 from the front surface to the maximum depth. When plotted as a function of displacement damage instead of helium concentration (Fig. 9), the two sets of data are in almost perfect agreement. Data from measurements on high-density SiC (SiC-HD from Elektroschmelzwerk Kempten, Germany) are included in Fig. 9 [19]. For consistency, the displacement values of these data were recalculated by TRIM95 (giving by a factor of about 2.2 higher values than used in Ref. [19]). Annealing experiments indicate that defects in SiC/C are immobile up to about 300 °C [20]. For immobile defects, the dose dependence of ε_0 can be described by a model for spontaneous recombination [21]

$$\varepsilon_0 = \frac{V_F}{3} \cdot \frac{Kt}{1 + v_r \cdot Kt}, \tag{6}$$

with V_F the volume dilatation per defect (formation volume) and v_r the instability volume around a defect (recombination volume) in units of atomic volumes Ω ($\Omega \approx 1.04 \times 10^{-29}$ m^3). A fit to the present data at ⩽70 °C (Fig. 9, dashed line) gives $V_F = 1.2$ and $v_r = 50$.

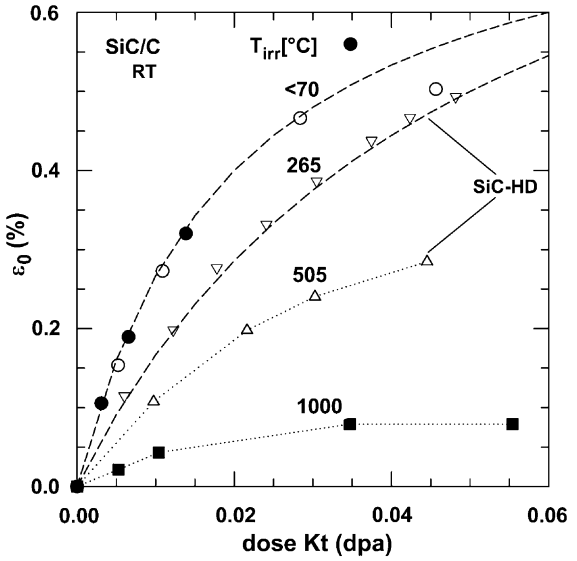

Fig. 9. Strains calculated from Eq. (6) from bending angles α (Fig. 5) for SiC/C specimens homogeneously implanted below 70 °C to depth of 117 μm (○) and 254 μm (●) and at 1000 °C to 254 μm (■), respectively. Included are strain data from SiC-HD proton-irradiated at 265 °C (▽), and 505 °C (△) without implantation [19]. The dashed lines give fits of Eq. (6); dotted lines are included to guide the eyes.

These values are in the same range as observed for metals but must be considered – as the above value of T_d – as averages for the different atomic species and components. In any case, absolute values mainly of V_F suffer from possible errors in the calculations of Kt, due to uncertainties in T_d. The 265 °C data from Ref. [19] can also be fitted by Eq. (6) by correcting the doses Kt by a factor f_{cp} which accounts for close-pair defects, which recombine already during implantation. The dashed line in this case gives (for $V_F = 1.2$) $f_{cp} = 0.5$ and $v_r = 20$. This decrease of v_r with increasing temperature is in accord with observations in metals [22,23]. The defect dynamics becomes rather complex at higher temperatures, with long-range migration of interstitials and vacancies of both C and Si and formation of various clusters in the different components, cf. [20]. These clusters, which are expected to have sizes in the nm range, could not be analysed by electron microscopy in the composite material, due to the complex microstructure, and therefore could not be included in the model calculations.

5. Summary

1. The apparent fracture stress in implanted SiC/C decreases with increasing helium concentration.
2. If irradiation-induced internal stresses are taken into account, fracture strength in the implanted region seems to be slightly increased, in comparison to the unimplanted matrix.
3. Straining in the implanted region is mainly due to displacement defects, while contributions of implanted helium are negligible.

References

[1] P. Jung, H. Schroeder, J. Nucl. Mater. 185 (1991) 149.
[2] P. Jung, J. Nucl. Mater. 191–194 (1992) 377.
[3] V.N. Chernikov, W. Kesternich, H. Ullmaier, J. Nucl. Mater. 227 (1996) 157.
[4] J.P. Biersack, L.G. Haggmark, Nucl. Instrum. and Meth. 174 (1980) 257.
[5] H.C. Smith, Carbon 1 (1964) 147.
[6] J.E. Brocklehurst, in: P.L. Walker, P.A. Thrower (Eds.), Chemistry and Physics of Carbon, vol. 13, Marcel Dekker, NY, 1977, p. 145.
[7] R.A. Matheny, J.C. Corelli, G.G. Trantina, J. Nucl. Mater. 83 (1979) 313.
[8] W. Dienst, J. Nucl. Mater. 191–194 (1992) 555.
[9] R.B. Matthews, W.G. Hutchings, J. Nucl. Mater. 45 (1972/1973) 341.
[10] R.B. Matthews, J. Nucl. Mater. 51 (1974) 203.
[11] N.M. Ghoniem, J. Nucl. Mater. 191–194 (1992) 515.
[12] P. Jung, Z. Zhu, J. Chen, J. Nucl. Mater. 251 (1997) 276.
[13] H.B. Müller, FZ Jülich – ZAT, private communication.
[14] H.W. Scholz, P. Fenici, A.F. Rebelo, Miniaturized specimens for testing of irradiated materials, in: P. Jung, H. Ullmaier (Eds.), IEA Int. Symp. Jülich (1994) 201.
[15] T. Stoto, L. Zuppiroli, in: P. Vincenzini (Ed.), High Tech Ceramics, Elsevier, 1987, p. 2959.
[16] C.G. Collins, J. Nucl. Mater. 14 (1964) 69.
[17] A. Kelly, N.H. MacMillan, Strong Solids, 3rd Ed., Clarendon, 1986.
[18] K. Abe, Report on the US–Japan workshop on 'small specimen testing techniques', Tokyo, JAERI Department of Fuels and Materials Research, 1988, p.107.
[19] Z. Zhu, P. Jung, J. Nucl. Mater. 212–215 (1994) 1081.
[20] J. Chen, P. Jung, H. Klein, J. Nucl. Mater. 258–263 (1998) 1803.
[21] Z. Zhu, P. Jung, Radiat. Eff. Def. Solids 144 (1998) 85.
[22] R. Lennartz, F. Dworschak, H. Wollenberger, J. Phys. F 7 (1977) 2011.
[23] U. Theis, H. Wollenberger, J. Nucl. Mater. 88 (1980) 121.